The Effect of Metals on Zeolite Crystallization Kinetics with Relevance to Nuclear Waste Glass Corrosion

James Neeway (James.Neeway@pnnl.gov)
Pacific Northwest National Laboratory https://orcid.org/0000-0001-7046-8408
Joelle Reiser
Pacific Northwest National Laboratory
Giannis Mpourmpakis
University of Pittsburgh
Radha Motkuri
Pacific Northwest National Laboratory https://orcid.org/0000-0002-2079-4798
Adam Mallette
University of Houston
Jeffrey Rimer
University of Houston

Article

Keywords: zeolite synthesis, crystallization, glass corrosion, nuclear waste

Posted Date: October 5th, 2022

DOI: https://doi.org/10.21203/rs.3.rs-2114477/v1

Version of Record: A version of this preprint was published at npj Materials Degradation on January 12th, 2023. See the published version at https://doi.org/10.1038/s41529-022-00310-9.

Abstract

Vitrification and geologic disposal of radioactive material is planned in several countries, but there are remaining uncertainties related to the long-term stability of glass exposed to groundwater. Specifically, the crystallization of aluminosilicate zeolite minerals can accelerate the rate at which glass corrodes and radioactive material is released into the biosphere. In this study, we identify elemental species that may accelerate or suppress zeolite formation using a protocol to examine their effects on zeolite synthesis over a three-day duration. Our results are consistent with previous works demonstrating glass corrosion acceleration in the presence of calcium. Furthermore, we identify two elements – tin and lithium – as inhibitors of zeolite P2 (GIS type, or gismondine) nucleation and, thus, promising species for promoting the long-term durability of glass waste forms.

Introduction

Radionuclides from nuclear waste can be incorporated into borosilicate glass matrices via vitrification to limit their release into the environment after geological disposal. To date, a wide range of proposed or actual glass compositions have been developed, which corrode at various rates upon exposure to water. In general, glasses corrode rapidly at first (Stage I) before dissolution rates are reduced to a much slower and (nearly) constant level (Stage II)[1,2]. In some cases, however, as the duration of the experiment increases, zeolite crystals are formed, whereupon the rate of glass dissolution precipitously increases (Stage III)[3–7]. Several zeolites either have been identified once a glass demonstrates Stage III behavior or are known to induce Stage III behavior when added to the system, including framework types CHA, ANA, and GIS (the three-letter codes refer to crystal structures designated by the International Zeolite Association). The focus of this study is to understand which oxides in the glass affect (either enhance or inhibit) the formation of zeolitic phases that result in Stage III dissolution behavior.

A vast array of oxides is used in glass formulations, but deconvoluting which elements promote or suppress zeolite nucleation remains challenging. In zeolite synthesis research, various elements in growth mixtures are understood to have distinct and significant effects on crystallization which are briefly surveyed here to summarize reported effects of elements known to alter zeolite formation. Besides Si and Al, which comprise the basic building blocks of natural and most synthetic zeolites, alkali metals are common extra-framework elements in zeolites. Indeed, these ions are often required to achieve fully crystalline products for many framework types because they balance negatively-charged AlO_4^- framework sites[8–14]. Alkali cations also function as structure-directing agents (SDAs) to facilitate the formation of a particular structure[14]. For instance, Kirschhock and coworkers[15] demonstrated that the product of seeded zeolite syntheses can be controlled simply by exchanging alkali cations (Li^+, Na^+, K^+, Rb^+, and Cs^+). Previously, the composition space of zeolites that form in sodium[8] and potassium[3] media has been mapped. Compared to alkali metals, alkaline earth metals (Group II) are rarely used as SDAs in zeolite synthesis; however, these cations are often present in natural zeolites, suggesting their influential role in geologic zeolite formation[16,17]. For instance, calcium[18], magnesium[19] and strontium[20] have each

been shown to increase zeolite crystallization rates. Compared to cations, anionic halides (Group VII) have a minimal effect on zeolite syntheses[14,21] with one exception: fluoride – which can replace hydroxide as a mineralizing agent (i.e., zeolite accelerant) that facilitates crystal formation with fewer defects[22–28]. The motive for adding elements in the transition metal block and groups III-V to the growth mixture is generally to isomorphically substitute heteroatoms (e.g., Zn, Sn, and Ga) into the crystal structure to enhance catalytic activity. These elements can have diverse effects on zeolite crystallization, which tends to be highly sensitive to the presence of inorganic additives. For example, small amounts of tin (Si/Sn molar ratio = 100) and zinc (Si/Zn molar ratio = 50) can extend the time required to synthesize zeolites BEA[29] and FAU[13], respectively, while germanium can accelerate the synthesis time for various framework types[30]. Owing to the complexity of zeolite synthesis mixtures, the underlying mechanistic causes of these phenomena are typically challenging to deconvolute.

To elucidate the effects of certain elemental oxides on glass corrosion, Crum et al.[31] designed a matrix of 24 waste glasses (Table S1) called the enhanced low-activity waste (eLAW) matrix. In particular, the matrix was subjected to a series of tests where zeolite P2 (GIS type, or gismondine) seeds were added to the glass-water system at pre-determined durations to help understand the propensity for various glass compositions to exhibit induced Stage III behavior. The statistically-designed matrix was developed for compositions pertinent to the Hanford Waste Treatment and Immobilization Plant (WTP)[32]. Seven major components (Al_2O_3, B_2O_3, CaO, Na_2O, SiO_2, SnO_2, and ZrO_2) were varied independently, while all remaining species were grouped into an eighth component (listed generically as “others”), which was also varied. The matrix was designed such that the individual effects of the seven major components and *others* could be isolated. In the study by Crum et al.[31], each of the 24 glasses was allowed to react with deionized water at 90°C in a stainless steel vessel for 28 days. Then, seeds of zeolite P2 (GIS type) were added to the system and the experiment continued at 90°C to observe whether or not the presence of the zeolite seeds affected the glass dissolution rate over the following twelve months. The addition of zeolite seeds has the potential to induce Stage III glass behavior on reasonable time scales[7], and zeolite P2 is used because it is one of the most common zeolites known to induce Stage III glass behavior[33]. Zeolite P2 is one of two common polymorphs possessing the GIS framework; the other is P1 (Fig. 1a), which is differentiated by a slight twist in the channel geometry that has been described in detail elsewhere[13,34]. Crum et al.[31] distinguished 4 types of glass behaviors depending on their composition: (Type 1) no effect of the seed, (Type 2) an immediate increase in the glass dissolution rate until all of the glass dissolved, (Type 3) an immediate increase in the glass dissolution followed by an eventual slowing in the rate, and (Type 4) an increase in the glass dissolution rate that was offset with respect to the time that the seeds were added. Most significantly, glasses with low calcium content resisted Stage III behavior significantly better than those with relatively high calcium content.

Though previous observations have been helpful in identifying the glass compositions that may be susceptible to Stage III dissolution behavior, the role of zeolite crystallization kinetics is still unclear as the zeolite seeds were added to the system, thus bypassing nucleation. Herein, we attempt to isolate the role

of crystallization kinetics by simulating the glass composition in solution (except for Na_2O, which was added in excess to attain a high solution pH) and identifying the resulting zeolite-containing product. This method allows us to bypass certain experimental constraints in the glass dissolution tests and isolate the role of select zeolite accelerants and suppressors. Herein, we investigate the consequences of various elements on zeolite crystallization kinetics in conventional synthesis mixtures. Selecting elements present in waste glass at higher compositions, we perform systematic studies using zeolite synthesis mixtures that more accurately replicate the glass composition. We show that modifications to zeolite growth mixtures by alkali metal substitution and/or alkaline earth metal addition can significantly alter crystallization rates. This approach aids the identification of certain glass compositions that may be susceptible to Stage III behavior in the environment and allow nuclear disposal facilities to potentially mitigate the effects of possible Stage III behavior due to zeolite crystallization.

Results And Discussion

The effects of many elements present in eLAW glass compositional matrix were investigated by adding each to a conventional synthesis[34] of zeolite P2 (GIS), one of the most common frameworks observed as an accelerant of nuclear waste glass dissolution rates (Fig. 1a)[35]. Synthesis mixtures have a molar composition of 9 SiO_2:0.5 Al_2O_3:5.5 Na_2O:0.2 M_xO_y:190 H_2O (where M = metal, x = number for M atoms, and y = number of O atoms) and were treated for 3 days at 100°C, which is sufficient for complete crystallization of GIS, by way of a FAU pathway, in a conventional zeolite synthesis (i.e., M = 0, Fig. S1). The hydrothermal treatment temperature was selected to be consistent with well-characterized zeolite syntheses.[8,34] Bulk crystallization assays where Na is combined with a range of different metals demonstrate that many higher valence elements (e.g., Cr, B, Zn, Sn, Fe) suppress GIS formation (Fig. 2, blue and Fig. S2a). Most notably, tin and zinc completely inhibit GIS crystallization for longer than 28 days of heating. The presence of a small FAU impurity used to distinguish elements that do not appear to alter crystallization rates (Mg, Sr, Zr, and Mn, Fig. 2, yellow; and Fig. S2b) from those that accelerate the formation of zeolite products (notably, Na, Li, and Ca; Fig. 2, red; and Fig. S2c), in conventional growth media used to prepare GIS crystals[34].

Following the initial survey of elements under conditions that are typical of synthetic zeolites, we sought to explore the effect of different elements when synthesis mixtures more accurately reflect the complex environment of altered nuclear waste glass. Our assumption is that all glass components are released congruently from the glass into solution whereas it is well known that the release of species from the glass is incongruent in static dissolution tests. Additionally, the present set of experiments ignores the possible effect that an altered glass substrate may play in zeolite nucleation kinetics. For a basis, we selected the seven major components (Al, B, Ca, Na, Si, Sn, and Zr) present in the eLAW series of 24 glasses assayed by Crum et al.[31] In the study carried out by Crum et al.[31], observations after seeding (Fig. 3a) could be described with four different behaviors types (and general compositional trends): (Type 1) no effect of the seed (low CaO), (Type 2) an immediate increase in the glass dissolution rate until all of the glass dissolved (high CaO, Al_2O_3, and ZrO_2), (Type 3) an immediate increase in the glass dissolution

followed by an eventual slowing in the rate (high CaO, B_2O_3, low Al_2O_3), and (Type 4) an increase in the glass dissolution rate that was offset with respect to the time that the seeds were added (high CaO, Al_2O_3, low ZrO_2). These glass classification types were made based on the general composition properties of a group of glasses that behaved similarly in glass dissolution relationship. For instance, not every glass in the latter group (high CaO, Al_2O_3, low ZrO_2) necessarily has a high CaO content. For the zeolite syntheses, the appropriate molar ratios were calculated where several values (H_2O, OH, and Si based on previous studies[8,14]) were held constant to maintain consistency across synthesis mixtures (Tables S3 and S4). To assess the effects of changing molar ratios, we heated each of the 24 mixtures, labeled eLAW-*X* (*X* = 1–24, Table S2), for 7 days at 100°C. In most cases, we observed a mixture of amorphous and crystalline (both zeolitic and non-zeolitic) phases in the products. Quantitative analysis of crystalline phase(s) was performed by refining powder X-ray diffraction (PXRD) patterns with the software Topas (Fig. S3) using MgO as an internal standard. In most cases, the dominant zeolite phase is GIS, but in select cases we observed crystals of metastable zeolite frameworks FAU (Fig. 1b) and LTA (Fig. 1c) that often form at similar synthesis conditions[8,36–40]. Among non-zeolitic phases, the most prominent is burtite, or calcium hexahydroxystannate ($Ca[Sn(OH)_6]$), which varies in weight fraction across the syntheses where it was detected (Table S5). Other precipitated non-zeolitic phases include calcium hydroxide ($Ca(OH)_2$) and zirconium oxide (ZrO_2), but neither Ca nor Zr appeared to influence zeolite crystallization in these experiments since their composition in the growth mixture could not be correlated to the fraction of GIS product (Figs. S3 – S5).

The phase outcomes of 24 eLAW zeolite syntheses from this study produced several noteworthy correlations to the behaviors presented in Fig. 3a. First, these findings revealed that short (< 7 days) and facile experiments may be capable of quickly assessing the susceptibility of certain glass compositions to precipitate zeolites much more rapidly than glass dissolution tests, which are both time- and resource-intensive. Among the seven components investigated, we identified two (calcium and tin) that most significantly impact zeolite crystallization; the fraction of zeolite GIS is not directly correlated with any other element (Fig. S5). These observations corroborate the results reported by Crum et al.[31] which suggest higher calcium content promotes zeolite formation and Stage III behavior (Fig. 3a). Indeed, a significant increase in the fraction of zeolite GIS product is apparent as the amount of calcium in the growth mixture increases (Figs. 3b and S6). Synthesis mixtures with the lowest amount of calcium (Ca/Si < 0.1) led to largely amorphous products and/or metastable zeolite phases, which suggests that a longer time is required for GIS crystallization. Increasing the amount of calcium to intermediate levels (0.1 < Ca/Si < 0.2) led to a significant increase in the amount of zeolite GIS formed. High calcium content (i.e. Ca/Si > 0.2) may slightly decrease the relative amount of zeolite GIS, which may be related to the limited solubility of Ca^{2+} ions in alkaline solutions and the tendency to precipitate as $Ca(OH)_2$. This effect is particularly evident in the case of glasses with high Ca and Al content and low Zr content (Fig. 2a, red curve; see also Fig. S6). Our findings that calcium promotes the nucleation of zeolite GIS aligns with computational investigations by Mpourmpakis and coworkers[41], who demonstrated that calcium cations substantively enhance the thermodynamic favorability of (alumino)silicate oligomerization.

The precise effect of tin on these systems is more challenging to discern compared to calcium given that several experimental observations are in apparent contradiction. First, our findings reveal that there is no clear correlation between the initial tin composition and the fraction of zeolite GIS product (Fig. S5). The quantity of tin is, however, correlated with the amount of burtite in the solid product (Fig. 4a), which is not observed for other elements (Fig. S7). Burtite is a crystalline structure that contains calcium (Fig. 4b); therefore, we hypothesize that tin plays a minor role in the suppression of GIS by sequestering calcium in the form of a solid mineral where it cannot promote zeolite nucleation. To this end, we demonstrated that burtite crystallizes prior to zeolite phases (Fig. 4c), which agrees with previous findings[42] and supports our hypothesis that burtite formation reduces the amount of calcium available for promoting zeolite nucleation. In a standard static glass corrosion experiment, this phase may not be observed; however, tin may play a role in preventing the release of calcium into solution.

It is well-known that zeolite crystallization is commonly suppressed by the presence of tin[29,43–45] even in the absence of calcium, which we have confirmed using a conventional zeolite synthesis mixture (Fig. 2). In this analysis, we aimed to deconvolute the effects of tin and calcium by removing the latter from the growth mixture and comparing the result to a case where both calcium and tin were absent. We selected eLAW-21 for this study because it led to a large amount of GIS product (Fig. S3). For the control synthesis using tin- and calcium-free media, we observed the formation of a zeolite product predominantly comprised of GME (Fig. 5, pattern *i*), which has a structure (Fig. 1d) similar to that of GIS (Fig. 1a). When tin was added to the synthesis mixture, we observed a largely amorphous product (Fig. 5, pattern *ii*) with a minor zeolite LTA phase. Therefore, tin clearly suppresses zeolite crystallization in syntheses replicating glass compositions irrespective of calcium content. Notably, tin seemingly affects the propensity of zeolite nucleation to occur in glass solution systems wherein we posit two potential mechanisms for its mode of action: (i) tin sequesters calcium accelerants and/or (ii) stannosilicate oligomers scavenge silica to form species that are putatively less amenable to zeolite nucleation compared to aluminosilicates[45]. The fraction of GIS product is more directly correlated with the concentration of calcium than that of tin (Figs. 3 and S5). This is partly attributed to the relatively high Ca/Si ratio in zeolite growth mixtures, but is more likely due to tin favoring burtite crystallization over that of GIS, as reflected in the changing product distribution as a function of Sn/Ca ratio (Fig. 6).

In these studies, the P1 polymorph of zeolite GIS was observed. The prevalence of zeolite P1 in the present study is suspected to be due to the limited quantity of available Si species as prior research[34] has established that zeolite P1 preferentially nucleates rather than zeolite P2 at low Si/OH ratios. Owing to the highly viscous synthesis mixture and diversity of sol-gel species, most of the Si species present may not be available for nucleation, lowering the effective Si/OH ratio. Since previous glass dissolution studies showed similar responses regardless of whether zeolites P1 or P2 seeds were added to the system[33,46], the observed trends from this study would likely not substantively change if zeolite P2 were to nucleate rather than zeolite P1.

Sodium is the most common alkali metal used to promote zeolite synthesis, so its prevalence in many nuclear waste glass compositions suggests that the partial substitution of sodium with alternative alkali metals may enhance glass stability with respect to Stage III behavior. We used eLAW-21 (Table S2) as the basis for these syntheses since it leads to a product with a relatively high fraction of zeolite GIS. Increasing the sodium content in the growth mixture to 120% of its original value leads to minimal changes, as expected (Fig. 7, pattern *i*). When potassium is added to the synthesis mixture (Na/K = 5), a partial zeolite MER phase is observed in the product (Fig. 1e; and Fig. 7, pattern *ii*), which is consistent with conventional zeolite syntheses where K^+ directs MER formation under otherwise similar conditions as GIS. Given that Li^+ is known to promote zeolite ABW[15], its addition was expected to lead to a dual mixture of GIS and ABW. Contrary to expectations, adding lithium to the synthesis mixture (Na/Li = 5) led to a largely amorphous product with a relatively small quantity of zeolite GIS product (Fig. 7, pattern *iii*), as indicated by the higher background intensity of the normalized pattern. This result is particularly surprising since the addition of lithium to a similar synthesis using conventional conditions (i.e., in the absence of the extra components used to mimic the glass composition) accelerates GIS crystallization (Fig. S8). This suggests that lithium may be altering the physicochemical structure of amorphous precursors or the nature of calcium species in such a way that significantly inhibits zeolite nucleation. Collectively, this result illustrates the importance of using synthesis mixtures that isolate the impacts of individual elements better than the more complex environment surrounding nuclear waste glass. Furthermore, simple modifications to glass (or synthesis mixture) compositions can significantly reduce the likelihood of zeolite nucleation, with the potential to dramatically enhance the durability of waste glass.

Conclusions

Zeolite synthesis studies where crystals nucleate from a mixture designed to replicate expected glass compositions are a valuable and efficient tool in assessing the likelihood that zeolites will precipitate during glass corrosion experiments. Results presented herein correlate well with expectations based on prior dissolution studies,[31] where glasses with low calcium content were the least likely to have increased dissolution rates when zeolite seeds were added, even if the synthesis mixtures having a higher pH (~ 13) than typical glass corrosion experiments (~ pH 10). Although deconvoluting the effects of diverse species is challenging, chemical insights from this study can provide a basis for future work towards predicting nuclear waste glass stability in a disposal scenario. We identify calcium as an accelerant of zeolite GIS crystallization and both tin and lithium as inhibitors. Additional accelerants and inhibitors have also been identified in conventional zeolite synthesis mixtures, but the correlation between these syntheses and glass compositions is less clear (Fig. S8), especially in light of the retention of certain species in the alteration layer during glass corrosion. This information can be used as a guide to design nuclear waste glass compositions that may be less susceptible to Stage III behavior.

Insights from this study also benefit the zeolite synthesis community. The systematic way this study was conducted provides a unique strategy for investigating the effects of diverse species on zeolite

syntheses. Perhaps one of the more surprising aspects of these results is that some elements (i.e., Ca and Sn) have a dramatic effect on crystallization outcomes while others (i.e., Zr and B) do not appear to have a substantial effect. However, the findings for this system may not be generalizable to syntheses of other zeolite topologies. Future investigation will be necessary to broaden the scope of this research to develop a more holistic understanding of how heteroatoms and other additives alter crystallization mechanisms across the ever-expanding library of zeolite framework types.

Materials And Methods

Materials. The following reagents were used for zeolite synthesis as purchased without further purification: LUDOX AS-40 colloidal silica (40 wt% suspension in water), sodium aluminate (anhydrous), sodium hydroxide (98% pellets), sodium chloride (99.5%), lithium hydroxide (anhydrous, 98%), potassium hydroxide (> 85%), tin (IV) chloride pentahydrate, zirconium (IV) oxide, ammonium metavanadate, chromium chloride hexahydrate, manganese (II) nitrate tetrahydrate (97%), iron (III) chloride hexahydrate, zinc nitrate hydrate (98%), boric acid (99.5%), copper nitrate hydrate, magnesium hydroxide (95%), magnesium oxide (99.4%), calcium hydroxide (95%), strontium hydroxide octahydrate (95%), barium hydroxide octahydrate (95%), and zinc oxide (99.9%). Deionized (DI) water was produced with an Aqua Solutions© purification system.

Conventional zeolite synthesis. Growth mixtures were prepared with molar compositions 9 Si:1 Al:0.5 M:11 NaOH:190 H_2O where M represents Li, Na, K, Mg, Ca, Sr, Ba, Zr, V, Cr, Mn, Fe, Zn, Sn, Cl, or B. Growth solutions were prepared in a polypropylene (PP) bottle. First, sodium hydroxide and sodium aluminate were dissolved in DI water under 5 minutes of magnetic stirring. Next, the M containing reagent was added (except for the control, where M = 0) and stirred either for 10 min or until dissolved. Then, LUDOX AS-40 was added using a plastic pipette, whereupon the synthesis mixture coagulated. The gel was immediately shaken, then stirred for 24 h at room temperature using a magnetic stir bar. After this, the synthesis mixture was transferred to a 100°C oven for a period of heating between 0–7 days depending on zeolite types (Figure S1), where 3 days was the nominal time. The solid product was then recovered as follows. Synthesis mixtures were washed with DI water (30 g) and transferred to a centrifuge tube using a nickel spatula. After centrifugation (5 min, 13,000 rpm), the supernatant solution was decanted. This procedure was repeated twice more with ~ 40 g DI water. The gel product was dried overnight in an incubator (~ 60°C).

Zeolite syntheses designed to replicate glass environment. Growth mixtures were prepared with molar compositions 60.2 SiO_2:*a* Al_2O_3:*b* CaO:*c* ZrO_2:*d* B_2O_3:*e* SnO_2:30.1 Na_2O:1270 H_2O where *a, b, c, d*, and *e* are selected to achieve the glass compositions displayed in Table S2. The same approach for conventional zeolite synthesis was used for zeolite synthesis designed to replicate glass environments with a few procedural changes. Sodium hydroxide and sodium aluminate were dissolved first like in conventional synthesis, followed individually by boric acid, tin (IV) chloride pentahydrate, zirconium (IV) oxide, calcium hydroxide, and finally LUDOX AS-40 which immediately causes the mixture to coagulate.

The same procedure described above was performed on the resulting gel, and the resulting solid product was recovered in the same manner described above for conventional zeolite synthesis.

Materials characterization. Powder X-ray diffraction (XRD) patterns were collected on a Rigaku diffractometer using Cu Kα radiation (40kV, 40 mA). Data were collected with a step size of 0.02 (2θ) at a rate of 8.33 steps per second. Phase quantification was performed using the fundamental parameters approach using TOPAS software[2]. Magnesium oxide was mixed into each zeolite sample as an internal standard at ~ 10 wt% to normalize XRD patterns and determine the crystalline and amorphous fraction of each sample.

Declarations

Declaration of competing interest:

The authors declare that they have no known competing financial interests or personal relationships that could have appeared to influence the work reported in this paper.

Author contributions:

The project was conceived by JDR, JJN, RKM, and GM. All zeolite crystallization experiments were performed by AJM and JDR. Zeolite characterization and data analysis were performed by AJM, JTR, and JJN. The original draft of the manuscript was prepared by AJM and JDR, with feedback from JTR, JJN, RKM, and GM. All authors contributed to editing and finalizing the manuscript.

ORCID:

Adam J. Mallette: 0000-0002-8917-5821

Joelle T. Reiser: 0000-0002-2638-1580

Giannis Mpourmpakis: 0000-0002-3063-0607

Radha K. Motkuri: 0000-0002-2079-4798

James J. Neeway: 0000-0001-7046-8408

Jeffrey D. Rimer: 0000-0002-2296-3428

Acknowledgments:

This work was supported by the U.S. Department of Energy (DOE), Nuclear Energy University Program (DOE-NEUP) under grant number 18-15496. JDR received additional support from The Welch Foundation (grant number E-1794).

References

1. Gin, S. *et al.* An international initiative on long-term behavior of high-level nuclear waste glass. Materials Today **16**, 243–248 (2013).
2. Vienna, J. D., Ryan, J. V., Gin, S. & Inagaki, Y. Current understanding and remaining challenges in modeling long-term degradation of borosilicate nuclear waste glasses. International Journal of Applied Glass Science **4**, 283–294 (2013).
3. Van Iseghem, P. & Grambow, B. The long-term corrosion and modelling of two simulated Belgian reference high-level waste glasses. *MRS Online Proceedings Library (OPL)* **112** (1987).
4. Strachan, D. M. & Croak, T. L. Compositional effects on long-term dissolution of borosilicate glass. Journal of Non-Crystalline Solids **272**, 22–33 (2000).
5. Strachan, D. M. & Neeway, J. J. Effects of alteration product precipitation on glass dissolution. Applied Geochemistry **45**, 144–157 (2014).
6. Fournier, M., Gin, S. & Frugier, P. Resumption of nuclear glass alteration: state of the art. Journal of Nuclear Materials **448**, 348–363 (2014).
7. Neeway, J. J. *et al.* Acceleration of glass alteration rates induced by zeolite seeds at controlled pH. Applied Geochemistry **113**, 104515 (2020).
8. Maldonado, M., Oleksiak, M. D., Chinta, S. & Rimer, J. D. Controlling crystal polymorphism in organic-free synthesis of Na-zeolites. Journal of the American Chemical Society **135**, 2641–2652 (2013).
9. Lobo, R. F., Zones, S. I. & Davis, M. E. Structure-direction in zeolite synthesis. Journal of Inclusion Phenomena and Molecular Recognition in Chemistry **21**, 47–78 (1995).
10. Asselman, K. *et al.* Super-ions of sodium cations with hydrated hydroxide anions: inorganic structure-directing agents in zeolite synthesis. Materials Horizons **8**, 2576–2583 (2021).
11. Shin, J., Jo, D. & Hong, S. B. Rediscovery of the importance of inorganic synthesis parameters in the search for new zeolites. Accounts of Chemical Research **52**, 1419–1427 (2019).
12. Jain, R., Mallette, A. J. & Rimer, J. D. Controlling nucleation pathways in zeolite crystallization: seeding conceptual methodologies for advanced materials design. Journal of the American Chemical Society **143**, 21446–21460 (2021).
13. Mallette, A. J. *et al.* Heteroatom Manipulation of Zeolite Crystallization: Stabilizing Zn-FAU against Interzeolite Transformation. JACS Au, doi:10.1021/jacsau.2c00325 (2022).
14. Chawla, A. *et al.* Crystallization of potassium-zeolites in organic-free media. Microporous and Mesoporous Materials, 112026 (2022).
15. Van Tendeloo, L., Gobechiya, E., Breynaert, E., Martens, J. A. & Kirschhock, C. E. A. Alkaline cations directing the transformation of FAU zeolites into five different framework types. Chemical Communications **49**, 11737–11739 (2013).
16. Pabalan, R. T. & Bertetti, F. P. Cation-exchange properties of natural zeolites. Reviews in Mineralogy and Geochemistry **45**, 453–518 (2001).

17. Khodabandeh, S. & Davis, M. E. Zeolites P1 and L as precursors for the preparation of alkaline-earth zeolites. Microporous Materials **12**, 347–359 (1997).
18. Xu, B., Smith, P., Wingate, C. & De Silva, L. The effect of calcium and temperature on the transformation of sodalite to cancrinite in Bayer digestion. Hydrometallurgy **105**, 75–81 (2010).
19. Lee, Y.-J., Lee, J. S. & Yoon, K. B. Synthesis of long zeolite-L crystals with flat facets. Microporous and Mesoporous Materials **80**, 237–246 (2005).
20. Liang, Y., Jacobson, A. J. & Rimer, J. D. Strontium ions function as both an accelerant and structure-directing agent of chabazite crystallization. ACS Materials Letters **3**, 187–192 (2020).
21. Cocks, P. A. & Pope, C. G. Salt effects on the synthesis of some aluminous zeolites. Zeolites **15**, 701–707 (1995).
22. Zones, S. I. *et al.* The fluoride-based route to all-silica molecular sieves; a strategy for synthesis of new materials based upon close-packing of guest–host products. Comptes Rendus Chimie **8**, 267–282 (2005).
23. Zones, S. I., Darton, R. J., Morris, R. & Hwang, S.-J. Studies on the role of fluoride ion vs reaction concentration in zeolite synthesis. The Journal of Physical Chemistry B **109**, 652–661 (2005).
24. Vattipalli, V., Paracha, A. M., Hu, W., Chen, H. & Fan, W. Broadening the Scope for Fluoride-Free Synthesis of Siliceous Zeolites. Angewandte Chemie International Edition **57**, 3607–3611 (2018).
25. Guth, J. L. *et al.* (ACS Publications, 1989).
26. Jon, H., Lu, B., Oumi, Y., Itabashi, K. & Sano, T. Synthesis and thermal stability of beta zeolite using ammonium fluoride. Microporous and Mesoporous Materials **89**, 88–95 (2006).
27. Camblor, M. A., Corma, A. & Valencia, S. Synthesis in fluoride media and characterisation of aluminosilicate zeolite beta. Journal of Materials Chemistry **8**, 2137–2145 (1998).
28. Eilertsen, E. A., Arstad, B., Svelle, S. & Lillerud, K. P. Single parameter synthesis of high silica CHA zeolites from fluoride media. Microporous and Mesoporous Materials **153**, 94–99 (2012).
29. Tolborg, S. *et al.* Incorporation of tin affects crystallization, morphology, and crystal composition of Sn-Beta. Journal of Materials Chemistry A **2**, 20252–20262 (2014).
30. Opanasenko, M. *et al.* Synthesis and Post-Synthesis Transformation of Germanosilicate Zeolites. Angewandte Chemie International Edition **59**, 19380–19389 (2020).
31. Crum, J. V. *et al.* Seeded Stage III glass dissolution behavior of a statistically designed glass matrix. Journal of the American Ceramic Society **104**, 4145–4162 (2021).
32. Russell, R. L. *et al.* Enhanced Hanford Low-Activity Waste Glass Property Data Development: Phase 2 PNNL-28838 Rev 2 (Pacific Northwest National Lab.(PNNL), Richland, WA (United States), 2021).
33. Parruzot, B. *et al.* Effect of zeolite type, temperature, and pH on Stage III glass alteration behavior for two nuclear waste glasses Journal of Nuclear Materials **567** (2022).
34. Oleksiak, M. D. *et al.* Synthesis strategies for ultrastable zeolite GIS polymorphs as sorbents for selective separations. Chemistry–A European Journal **22**, 16078–16088 (2016).

35. Fournier, M., Gin, S., Frugier, P. & Mercado-Depierre, S. Contribution of zeolite-seeded experiments to the understanding of resumption of glass alteration. npj Materials Degradation **1**, 1–13 (2017).
36. Conato, M. T., Oleksiak, M. D., McGrail, B. P., Motkuri, R. K. & Rimer, J. D. Framework stabilization of Si-rich LTA zeolite prepared in organic-free media. Chemical Communications **51**, 269–272 (2015).
37. Sharma, P., Song, J.-S., Han, M. H. & Cho, C.-H. GIS-NaP1 zeolite microspheres as potential water adsorption material: Influence of initial silica concentration on adsorptive and physical/topological properties. Scientific Reports **6**, 1–26 (2016).
38. Fan, W., Shirato, S., Gao, F., Ogura, M. & Okubo, T. Phase selection of FAU and LTA zeolites by controlling synthesis parameters. Microporous and Mesoporous Materials **89**, 227–234 (2006).
39. Zhu, G. *et al.* Synthesis and characterization of high-quality zeolite LTA and FAU single nanocrystals. Chemistry of Materials **10**, 1483–1486 (1998).
40. Oleksiak, M. D., Soltis, J. A., Conato, M. T., Penn, R. L. & Rimer, J. D. Nucleation of FAU and LTA zeolites from heterogeneous aluminosilicate precursors. Chemistry of Materials **28**, 4906–4916 (2016).
41. Freeman, E. E., Neeway, J. J., Motkuri, R. K., Rimer, J. D. & Mpourmpakis, G. Understanding initial zeolite oligomerization steps with first principles calculations. AIChE Journal **66**, e17107 (2020).
42. Sonnet, P. M. Burtite, calcium hexahydroxostannate, a new mineral from El Hamman, central Morocco. The Canadian Mineralogist **19**, 397–401 (1981).
43. Lew, C. M., Rajabbeigi, N. & Tsapatsis, M. Tin-containing zeolite for the isomerization of cellulosic sugars. Microporous and Mesoporous Materials **153**, 55–58 (2012).
44. Kasula, M., Spanos, A. P., Ford, L. & Brunelli, N. A. Investigating the Impact of Synthesis Conditions to Increase the Yield and Tin Incorporation Efficiency for Lewis Acid Nano-Sn-MFI Zeolites. Industrial & Engineering Chemistry Research **61**, 1977–1984 (2022).
45. Kinrade, S. D., Syvitski, R. T., Marat, K. & Knight, C. T. G. Two-Dimensional Silicon-29/Tin-117 NMR Evidence of Aqueous Stannosilicate Anions. Journal of the American Chemical Society **118**, 4196–4197 (1996).
46. Parruzot, B. *et al.* Multi-glass investigation of Stage III glass dissolution behavior from 22 to 90 ^{o}C triggered by the addition of zeolite phases Journal of Nuclear Materials **523**, 490–501 (2019).

Figures

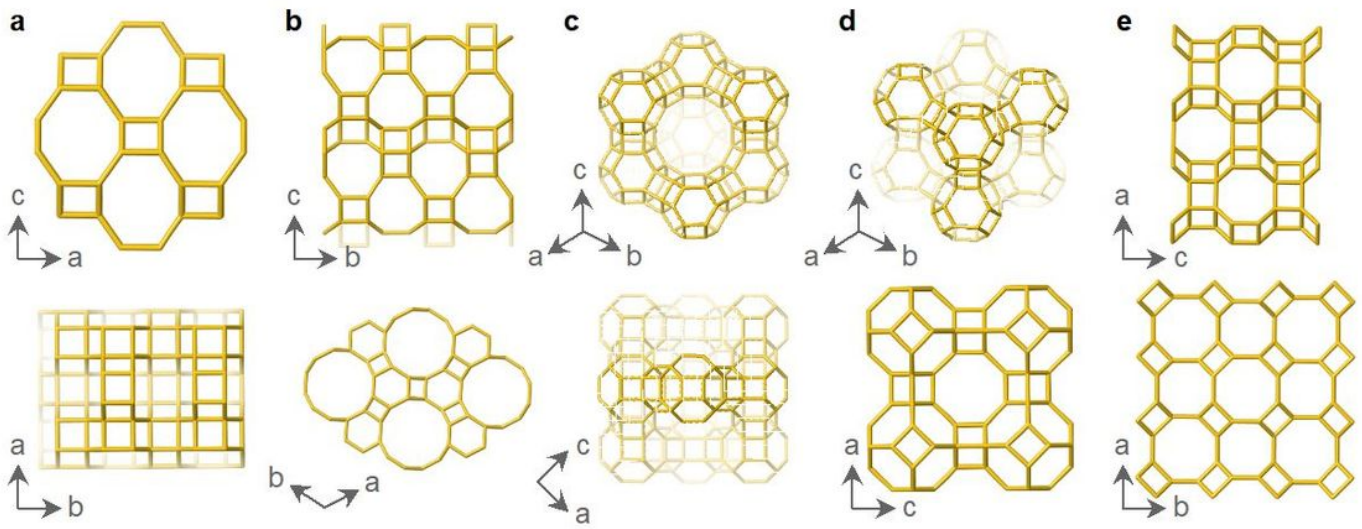

Figure 1

Zeolite frameworks. Crystal structures of zeolite framework types synthesized in this study: (a) GIS, (P1 polymorph) (b) FAU, (c) LTA, (d) GME, and (e) MER.

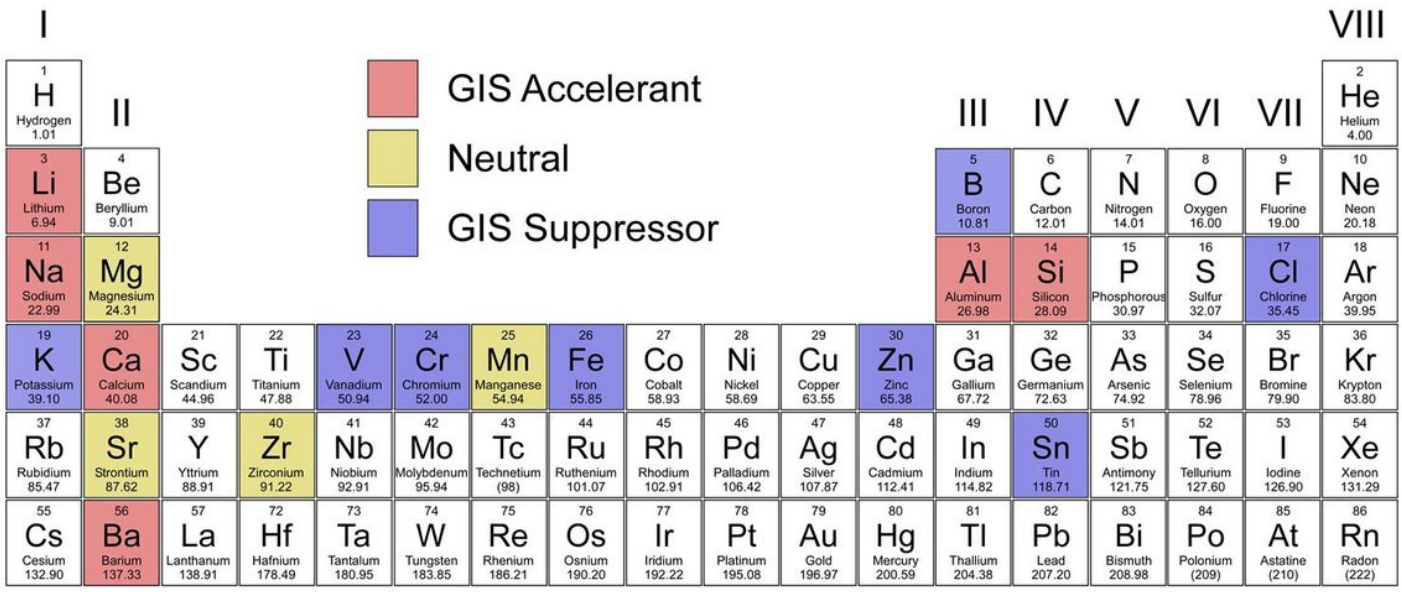

Figure 2

Periodic table. Effect of elemental species on zeolite GIS crystallization rates using conventional synthesis conditions. Each synthesis was carried out for 3 days at 100°C using a growth mixture with a molar composition of 9 SiO_2:0.5 Al_2O_3:5.5 Na_2O:0.2 M_xO_y:190 H_2O. Growth mixtures have a pH value of

~13. Reagent “M” corresponds to elements added (see Materials section for details), which is color-coded according to its effect on the crystallization rate: accelerant (red), suppressor (blue), or neutral (yellow).

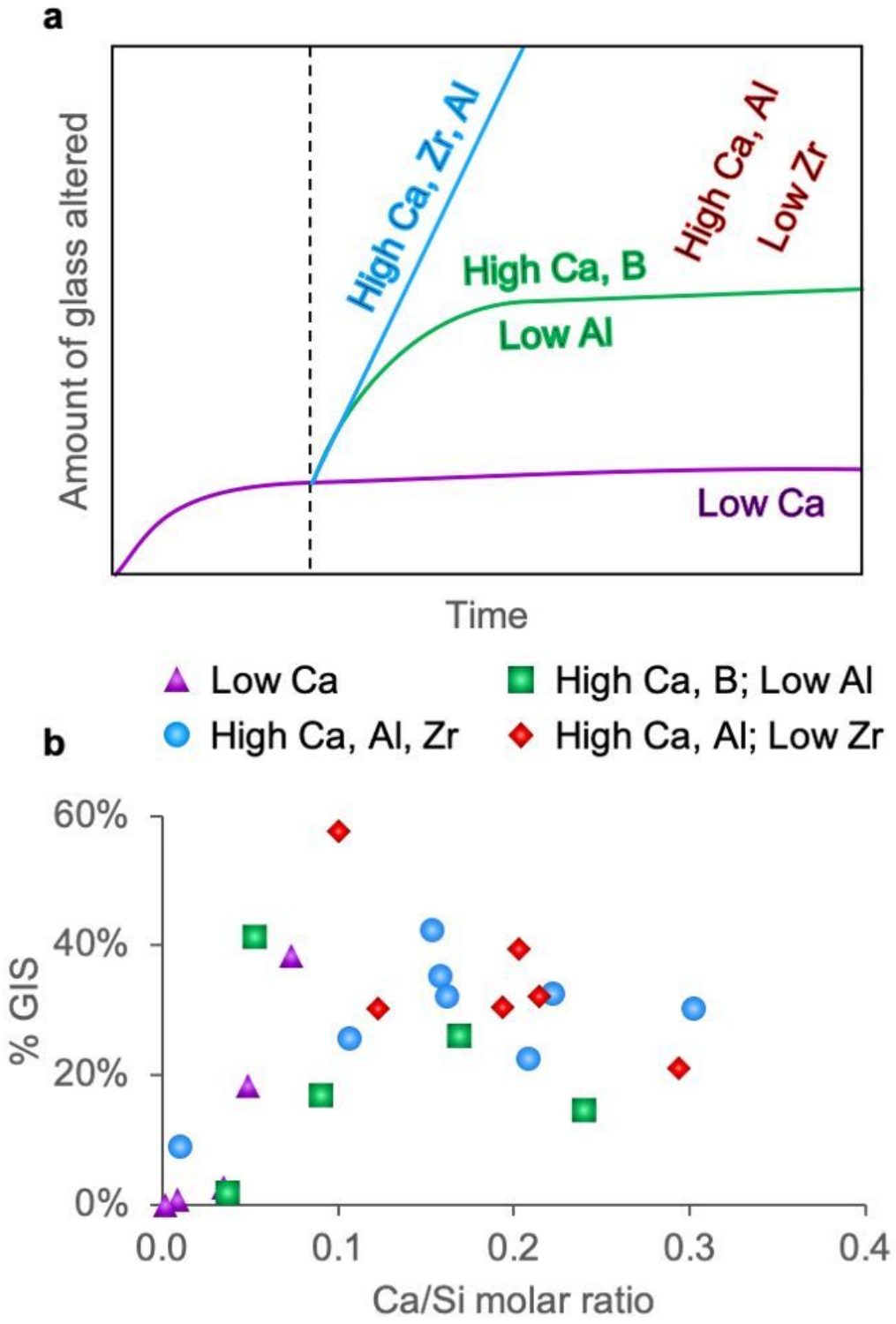

Figure 3

Effect of Ca. (a) Qualitative response curves of eLAW glasses in dissolution studies performed in the presence of zeolite seeds, as reported by Crum et al.[31]. Seed addition (dashed vertical line) allows for

glass responses to be assayed on a reasonable timeframe. Glasses are characterized and grouped according to their compositions: Type 1, low CaO (purple); Type 2, high Ca, Al, Zr (blue); Type 3, high Ca, B, and low Al (green); and Type 4, high Ca, Al, and low Zr (red). (b) Experimentally observed weight fraction of zeolite GIS phase in the product of bulk crystallization versus Ca/Si molar ratio in the initial synthesis mixtures designed to mimic eLAW glass conditions[31]. Exact molar compositions and product phase information are presented in Tables S2 and S5, respectively. Color coding of data points is based on the classification of each glass according to panel A, which corresponds to alteration responses for glasses with low CaO (purple triangles); high CaO, Al_2O_3, ZrO_2 (blue circles); high CaO, B_2O_3, and low Al_2O_3 (green squares); and high CaO, Al_2O_3, and low ZrO_2 (red diamonds).

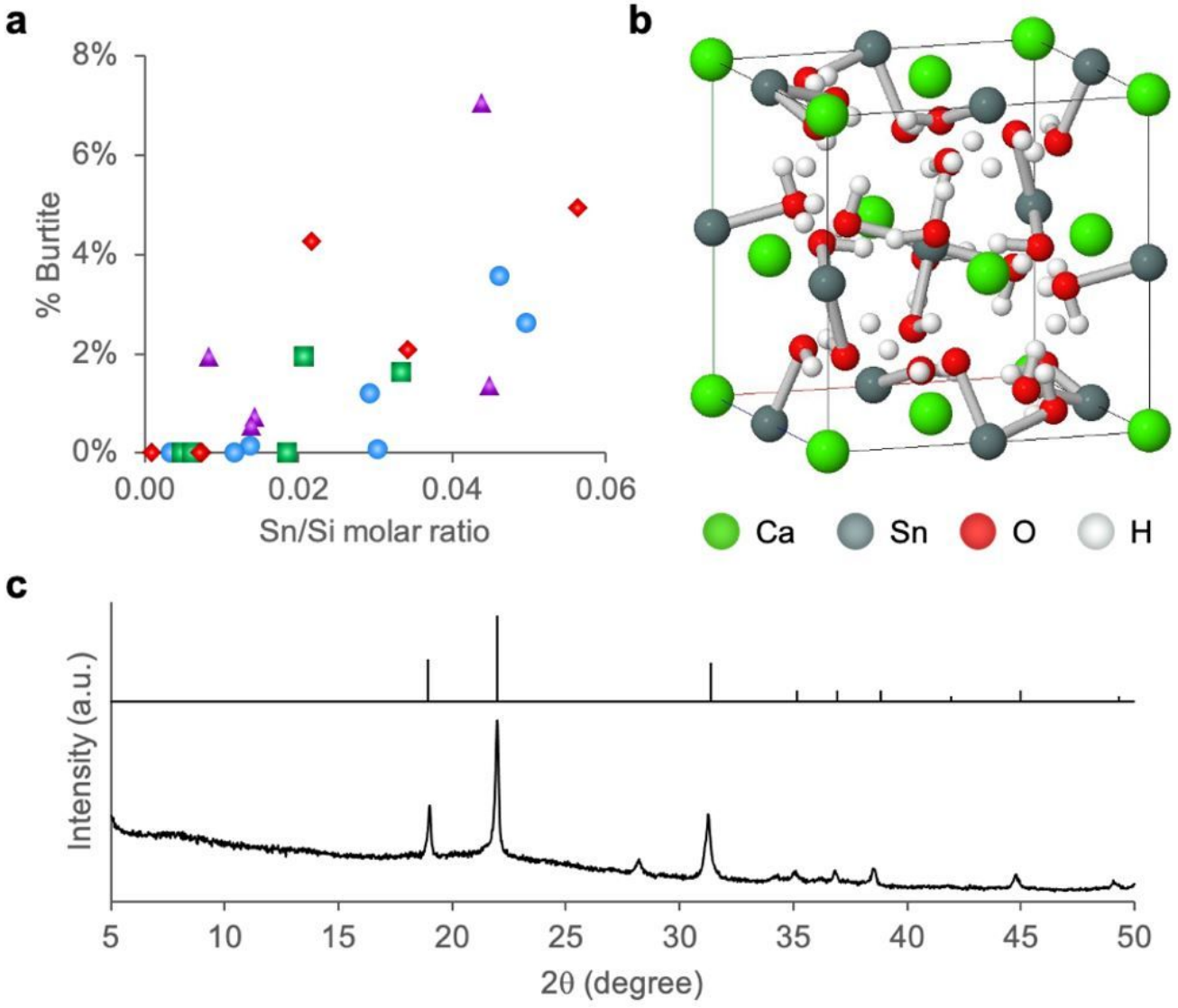

Figure 4

Effect of Sn. (a) Graphical relationship illustrating the positive correlation between the weight fraction of burtite in products of eLAW zeolite synthesis series and the amount of tin in the growth mixture. Refer to

the legend in Fig. 3B for symbol descriptions. (b) Burtite crystal structure, adapted with permission[42]. (c) PXRD pattern of burtite (bottom) synthesized by aging zeolite growth mixture eLAW-24 which had the highest Sn molar ratio (Table S2) for 24 h at room temperature without hydrothermal treatment. Reference pattern for burtite (top) was obtained from the American Mineralogist Crystal Structure Database.

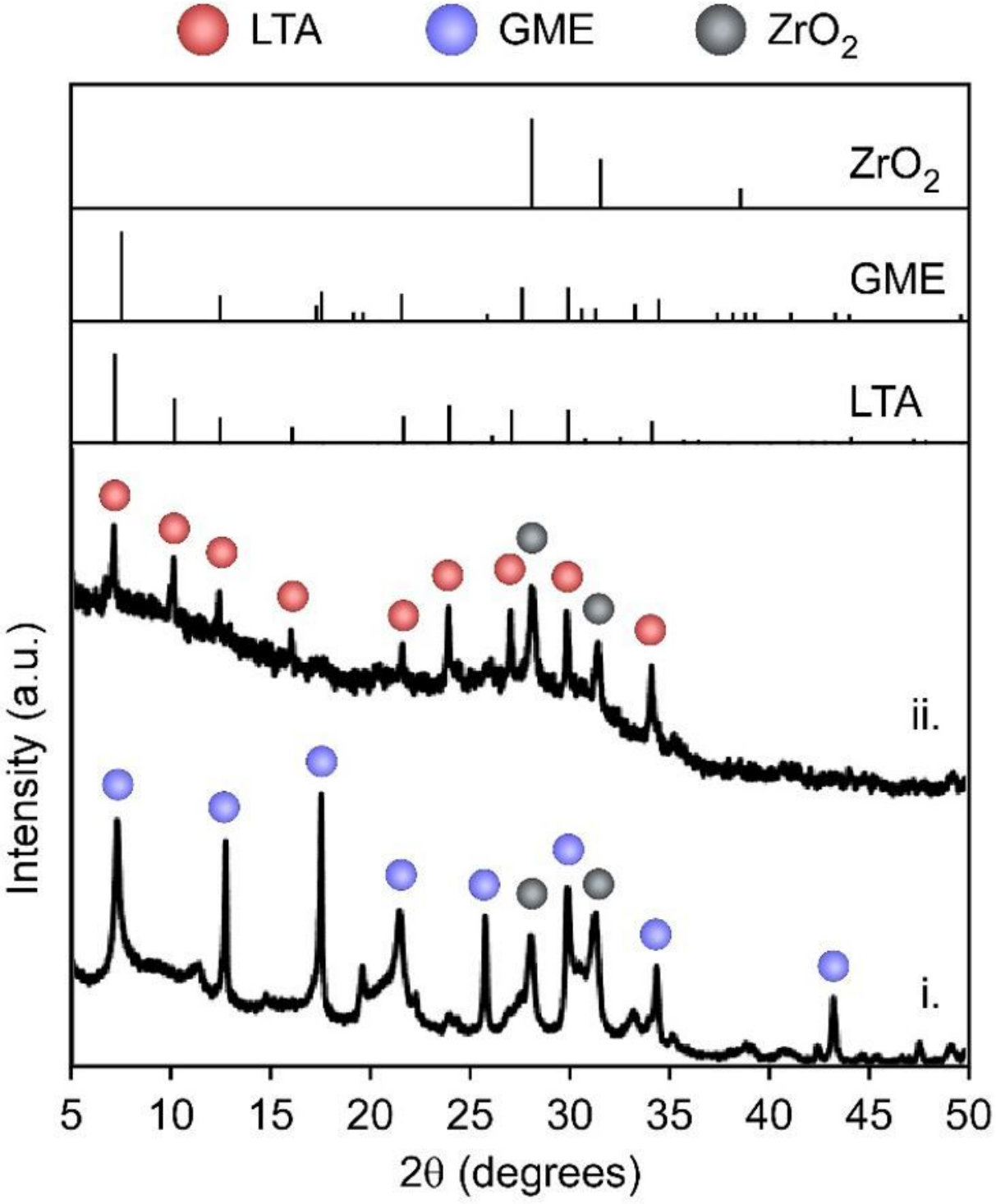

Figure 5

Deconvoluting Sn and Ca. PXRD patterns illustrating the effect of tin on samples synthesized with a molar composition similar to that of eLAW-21 (Table S2). (i) eLAW-21 synthesis repeated in the absence of Ca and Sn. (ii) eLAW-21 synthesis repeated in the absence of Ca and in the presence of Sn. Solid products were extracted from syntheses after 7 days at 100°C. Reference patterns of ZrO_2, GME, and LTA are provided. The PXRD pattern of solid generated from the original eLAW-21 synthesis is displayed in Fig. S3 for reference.

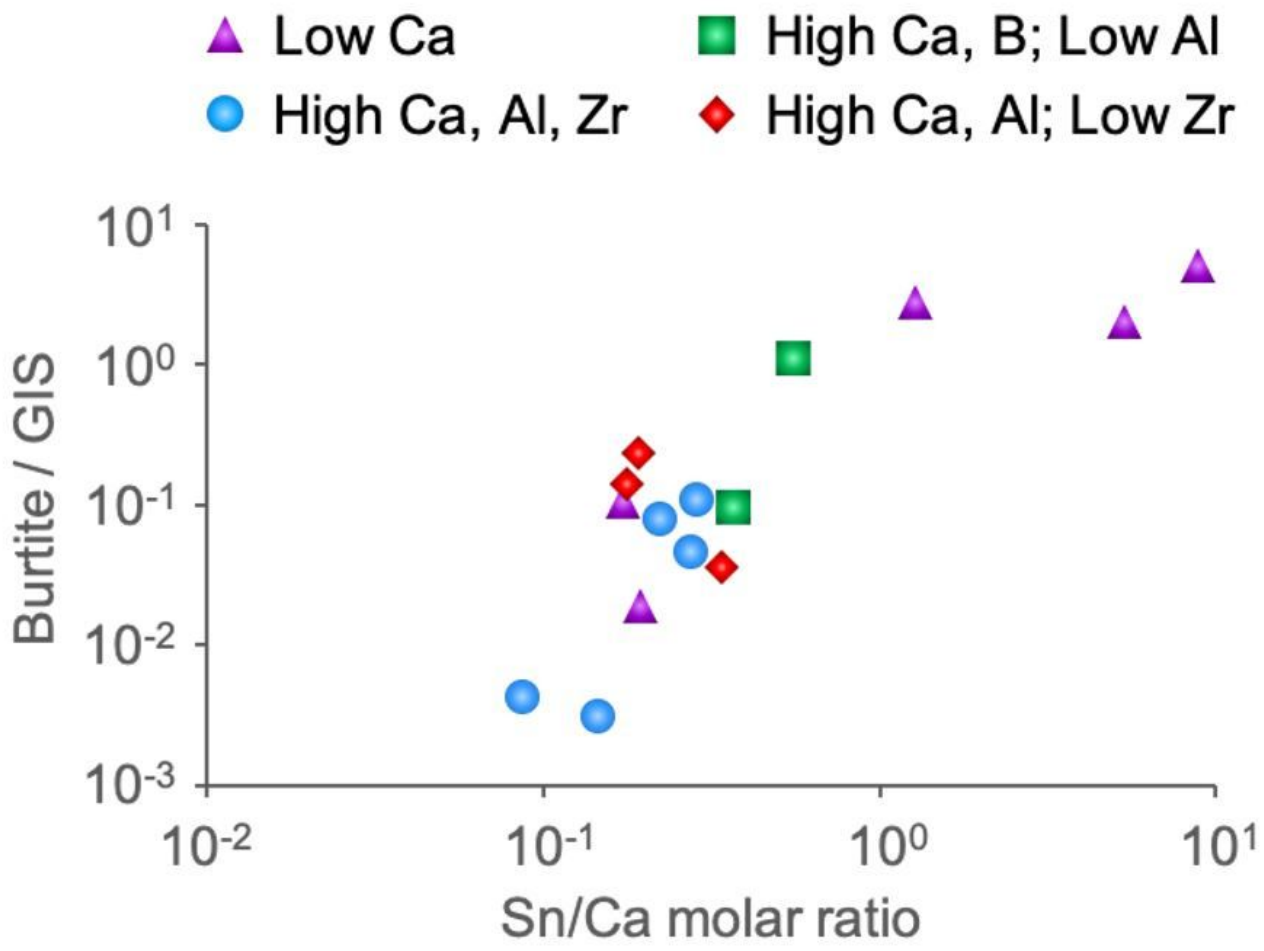

Figure 6

Effect of Sn/Ca ratio. Logarithmic relationship between the relative amounts of burtite and GIS by weight in the final product (calculated from PXRD patterns using MgO as an internal standard) as a function of the initial Sn/Ca molar ratio of the growth mixture. Color coding of data points is based on the classification of each glass according to Fig. 3a, which corresponds to alteration responses for glasses with low CaO (purple triangles); high CaO, Al_2O_3, ZrO_2 (blue circles); high CaO, B_2O_3, and low Al_2O_3 (green squares); and high CaO, Al_2O_3, and low ZrO_2 (red diamonds). Some samples are not plotted which do not contain a quantifiable amount of burtite according to their PXRD pattern.

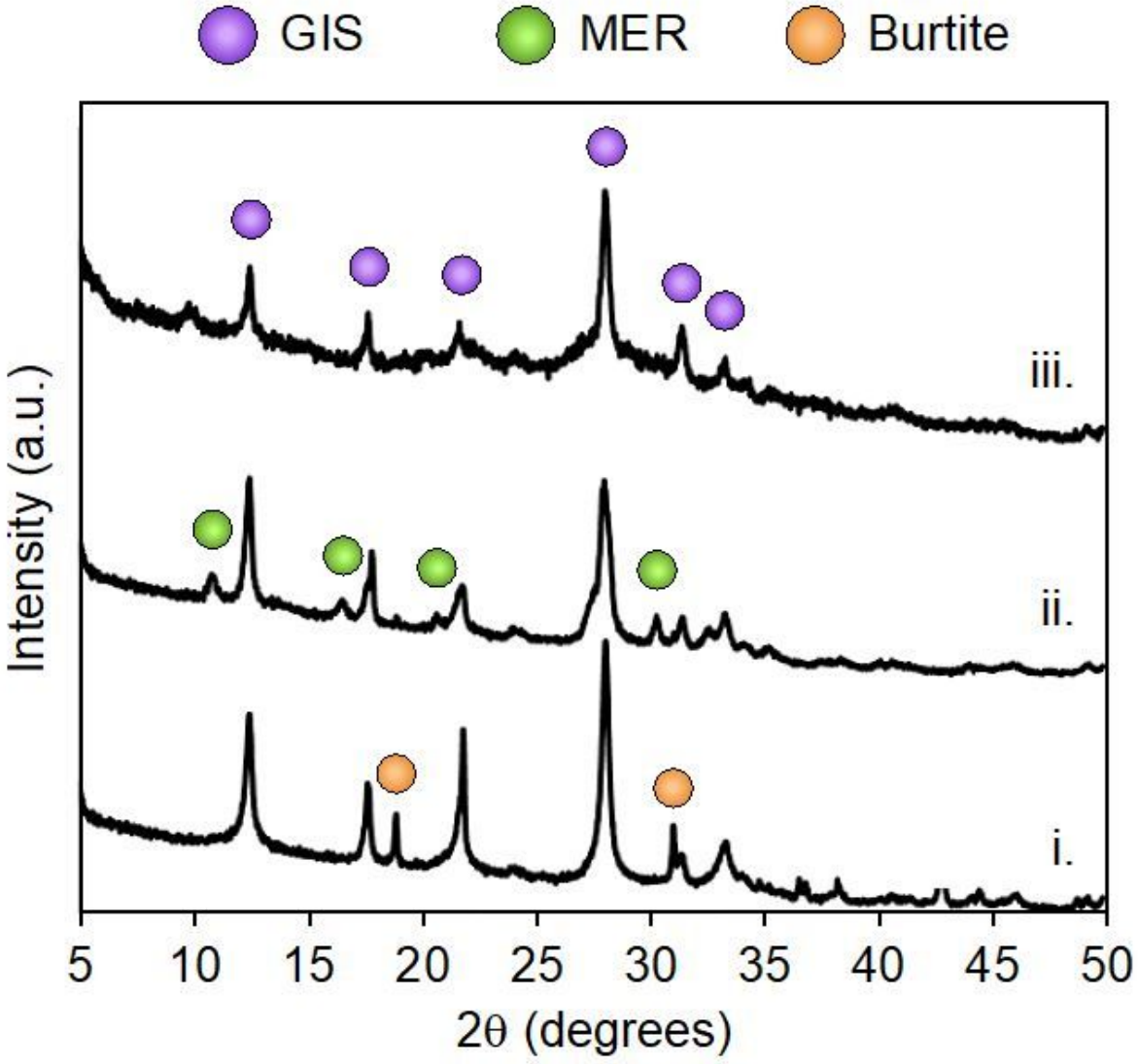

Figure 7

Alkali metal substitution. Normalized PXRD patterns of products generated from a synthesis mixture designed to replicate the glass composition of eLAW-21 (Table S2) with variations in the alkali metal content. Growth mixtures were prepared with molar compositions of 60.5 SiO_2:8.7 Al_2O_3:29.8 Na_2O:6 M_2O:11.2 B_2O_3:2.0 ZrO_2:6.1 CaO: 2.1 SnO_2:1270 H_2O where M = Na (i), K (ii), and Li (iii). All syntheses were carried out for 7 days at 100°C. Synthesis A contains 120% the amount of sodium present in eLAW-21. PXRD patterns are normalized for clarity.

Supplementary Files

This is a list of supplementary files associated with this preprint. Click to download.

- TOC.jpg

- MalletteSupportingInformation.docx